ACTA ASTRONOMICA
Vol. **61** (2011) pp. 199–216

The Optical Gravitational Lensing Experiment. High Proper Motion Stars in the OGLE-III Data for Magellanic Clouds Fields *

R. Poleski[1], I. Soszyński[1], A. Udalski[1],
M.K. Szymański[1], M. Kubiak[1], G. Pietrzyński[1,2],
Ł. Wyrzykowski[1,3] and K. Ulaczyk[1]

[1] Warsaw University Observatory, Al. Ujazdowskie 4, 00-478 Warszawa, Poland
e-mail: (rpoleski,soszynsk,udalski,msz,mk,pietrzyn,wyrzykow,kulaczyk)@astrouw.edu.pl
[2] Universidad de Concepción, Departamento de Fisica, Casilla 160-C, Concepción, Chile
[3] Institute of Astronomy, University of Cambridge, Madingley Road, Cambridge
CB3 0HA, UK

Received September 13, 2011

ABSTRACT

We present the results of a search for High Proper Motion (HPM) stars, *i.e.*, the ones with $\mu >$ 100 mas/yr, in the direction to the Magellanic Clouds. This sky area was not examined in detail as the high stellar density hampers efforts in performing high-quality astrometry.

Altogether 549 HPM stars were found with median uncertainties of proper motions per coordinate equal to 0.5 mas/yr. The fastest HPM star has the proper motion of 722.19 ± 0.74 mas/yr. For the majority of objects (70%) parallaxes were also measured. The highest value found is $\pi = 91.3 \pm 1.6$ mas. The parallaxes were used to estimate absolute magnitudes which enriched with color information show that 21 of HPM stars are white dwarfs. Other 23 candidate white dwarfs were selected of HPM stars with no measurable parallaxes using color–magnitude diagram. The search for common proper motion binaries revealed 27 such pairs in the catalog. The completeness of the catalog is estimated to be $> 80\%$ and it is slightly higher than for previous catalogs in the direction to the Magellanic Clouds.

Key words: *Astrometry – Catalogs – Stars: kinematics and dynamics – binaries: visual – white dwarfs*

1. Introduction

Previous surveys searching for High Proper Motion (HPM) stars typically avoided dense stellar regions of the Magellanic Clouds (MCs; *e.g.*, Finch *et al.* 2007 as a part of SuperCOSMOS-RECONS survey). First, high stellar density hampers HPM star

*Based on observations obtained with the 1.3 m Warsaw telescope at the Las Campanas Observatory of the Carnegie Institution for Science.

identification especially in two-epoch surveys. Second, the probability of blending of a HPM star with a background object which lowers the observed proper motion of the light centroid of both objects is high (Kozłowski *et al.* 2006). The SPM4 survey (Girard *et al.* 2011) covers the area of MCs, but it uses only two epochs and suffers from problems with star identification. To search for HPM objects Alcock *et al.* (2001) and Soszyński *et al.* (2002) used, respectively, the MACHO and the second phase of the Optical Gravitational Lensing Experiment (OGLE-II) surveys data, which both aimed at searching for microlensing events. In this paper we extend the study of Soszyński *et al.* (2002) using the data collected during the third phase of the OGLE survey (OGLE-III), which covered larger sky area (54 *vs.* 8.3 deg^2), longer time baseline (8 *vs.* 4 years) and had better pixel scale (0.26 *vs.* 0.46 arsec/pixel). Since the OGLE-III was a photometric survey, the observing strategy was not optimized for astrometry. However, the large number of epochs taken at good seeing conditions allowed us to measure proper motions and parallaxes at milliarcsecond level with milliarcsecond precision.

In Section 2 we describe observations and data reduction which was performed before we started this research. Sections 3 and 4 describe calculation of PM and selection of HPM objects. In Section 5 we describe the catalog, asses its completeness, compare with other catalogs, analyze color–absolute magnitude and color–magnitude diagrams (CMDs) as well as list common proper motion (CPM) binaries.

2. Observations and Initial Data Reduction

The OGLE-III observations were carried out between 2001 and 2009 with 1.3-m Warsaw telescope located at Las Campanas Observatory, Chile. The observatory is operated by the Carnegie Institution for Science. The only one instrument attached to the Warsaw telescope at that time was the "second generation" camera[†]. It consisted of eight 2048×4096 pixel CCD detectors with 15 μm pixels which gave 0.26 arcsec/pixel scale. The total field of view was 35×35.5 arcmin. Around 90% of the images of the MCs were taken with the *I* filter and the remaining with the *V* filter. We analyzed only *I*-band images number of which varied between 385 and 637 for the Large Magellanic Cloud (LMC) fields and between 583 and 762 for the Small Magellanic Cloud (SMC) fields with the exception of the field SMC128 for which 1228 epochs were secured. The time baseline was 4.5 yr for the field SMC140 (covering the center of the globular cluster 47 Tuc) and between 7.5 yr and 7.9 yr for the remaining fields. The details of the instrumentation setup were given by Udalski (2003).

Hardly ever a single MCs field was observed more than once per night during the OGLE-III survey. Centers of the observed fields were fixed and the only shifts

[†]Note that Anderson *et al.* (2006) found distortion corrections accurate to ≈ 7 mas for individual frames taken with WFI camera on 2.2-m ESO telescope and ≈ 100 mas changes caused by the manipulation of the camera.

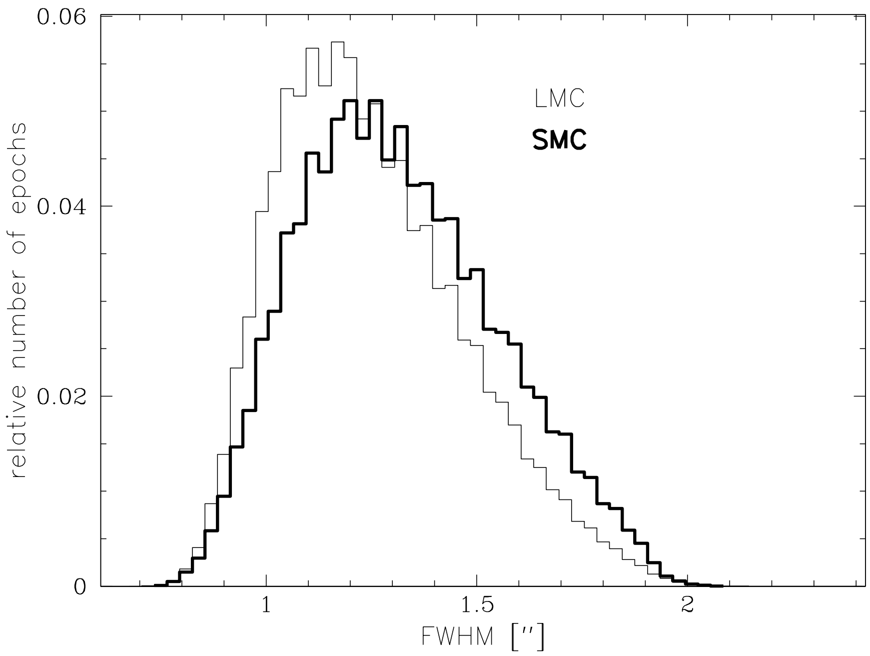

Fig. 1. Relative number of epochs taken with given FWHM of stellar profiles for LMC (thick line) and SMC (thin line) separately. The bin size is $0\rlap{.}''03$.

resulted from the telescope pointing errors. Fig. 1 shows the relative number of exposures for a range of seeing for the LMC and SMC fields separately. The median seeing was $1\rlap{.}''2$ and one can see a slightly worse seeing for SMC caused by the higher airmasses at which the images were taken. The minimum airmasses of the LMC and SMC fields during observations were 1.26 and 1.34, respectively. The images were taken at airmasses up to 2. The standard OGLE-III photometry was obtained with the Difference Image Analysis (DIA) method (Alard and Lupton 1998, Alard 2000, Woźniak 2000). DIA requires reference images which were constructed using up to 30 best images of a given field (Udalski *et al.* 2008a). The direct transformation from the pixel coordinates to the equatorial coordinates is available only for the reference images. The transformation was based on the Two Micron All Sky Survey (Skurstkie *et al.* 2006) catalog and gave $0\rlap{.}''12$, *rms* per coordinate when compared to the Third US Naval Observatory CCD Astrograph Catalog (Zacharias *et al.* 2010). The photometric maps of the MCs based on the OGLE-III reference images were published by Udalski *et al.* (2008b, 2008c).

The preparation of the reference images began with the selection of the best images for each subfield (which corresponds to a single CCD chip of the mosaic) separately. Each subfield was divided into two or eight subframes (the size was either 2180×2088 or 1090×1044 pixels) and analyzed separately. The images used for the reference image construction were resampled to the grid of the best quality subframe on the list. Before the resampling was done a cross-match was performed on the list of bright stars found on the given image and the reference image. For the MCs fields a typical brightness limit for stars used in the cross-matching was between 18 and 18.5 mag and depended on seeing, airmass, etc. Next, to find the transformation between the analyzed and the reference subframes, the third order polynomial was fitted. To remove outliers from the fit, 3σ-clipping was performed and a new set of polynomial coefficients were found. Then, the analyzed subframe was resampled to the reference grid using spline method and the polynomial found above. Finally, all the resampled subframes were co-added in the way that each pixel was composed of up to 10 pixels from the resampled subframes. The advantage of the spline resampling is that it conserves the total flux of each star.

Each individual image was divided into subframes corresponding to the subframes of the reference image, and each of them was resampled to the grid of the reference subframe. The procedure of calculating transformation and resampling was the same as described above. It allows the indirect calculation of the equatorial coordinates for each epoch separately. Further reduction for the standard OGLE photometry was performed using the DIA package. All the transformed images were also reduced using the DOPHOT software (Schechter *et al.* 1993) and this study is based on these data only. This additional reduction allows a simple selection of foreground Galactic objects based on the time series astrometry. The DOPHOT performs analytical model point spread function (PSF) fitting and was run in the spatially-variable PSF mode. The stellar positions measured on each image were associated with the stellar object on the reference image, where matching radius of 1.9 pixel was used. These data were used *e.g.*, to select Galactic variable stars in an on-going research of the OGLE-III Catalog of Variable Stars (*e.g.*, Soszyński *et al.* 2009 lists 66 Galactic RR Lyr type variables). For some stars (*e.g.*, the ones with brightness close to the saturation limit) the DOPHOT photometry is more robust than the DIA one. The details of the reference image construction and obtaining the DOPHOT photometry were described by Udalski *et al.* (2008a).

The procedure described above was far from being optimal for astrometric purposes. We describe their main disadvantages below. First, transformation of grids was performed on centroids found using one program (SFIND in this case; Woźniak 2000) and after the transformation was done the second time centroids were found using another program (DOPHOT). The results of both programs might be different. In the exceptional case we found a mean difference of 0.1 pixel and the inspection of the image revealed that even though the seeing was better than average the shape of the PSF was elongated and the DOPHOT treated each star as two separate objects, which affected measured centroids. Second, the transformation was calculated using all the bright stars, including HPM objects. Also very red or very blue objects affected calculated transformation, as the differential refraction effect was not removed. Third, the spline resampling does not conserve relative positions of centroids. This effect had very slight influence on the measured positions. Fourth, the measured centroids were cross-referenced with the database records with a constant radius, so the fastest HPM stars were at different epochs associated with the different database records. It was also because the reference images were constructed using the stellar positions from different epochs and HPM stars have elongated profiles or even the profiles have more than one local maximum.

With the last of the disadvantages mentioned we could cope, because the raw DOPHOT results were secured and can be queried around a certain position on the chip. Proper removing of the first two disadvantages was somewhat more complicated. It would require almost the entire reanalysis of a huge dataset. Instead of doing this very computer time consuming task we decided to apply a post-mortem corrections to the measured positions which reduced these effects. Even though we did not fully remove them our results gave very precise and reliable proper motions in the dense stellar fields.

3. Method of Proper Motion Calculation

The quantities which affect the position of the star and are important from astrophysical point of view are the proper motion and the parallax. Ground-based observations are also affected by the atmospheric refraction and the annual aberration. Telescope pointing removed aberration for the field center. For the wide-field imagers one also has to remove differential aberration caused by the difference in angular separation between Earth apex and different points of the sky imaged. In the OGLE-III pipeline differential aberration was removed by the resampling procedure described above. This also removed the mean atmospheric refraction. Refraction depends on the spectrum of an object, thus we had to take into account differential refraction. At time t ($t = 0$ for 2000.0) the observed position of the star (α, δ) is given by the following formulae:

$$\alpha = \alpha_0 + \mu_\alpha t + \frac{r \sin p \tan z + \pi \sin\gamma \sin\beta}{\cos\delta} \tag{1}$$

$$\delta = \delta_0 + \mu_\delta t + r \cos p \tan z + \pi \sin\gamma \cos\beta \tag{2}$$

where μ_α and μ_δ are proper motions along the right ascension and the declination. Differential refraction coefficient and parallax are designated r and π, respectively, z is the zenith distance, α_0 and δ_0 are coordinates for the J2000.0 equinox, γ is the angular distance to the Sun, β and p are angles between direction of parallax shift and refractional shift, respectively, and direction to the North celestial pole.

Kuijken and Rich (2002) showed that the uncertainty with which one measures the centroid of a star (σ_{PSF}) depends on the Full Width at Half Maximum (FWHM) of the stellar profile and the signal to noise (S/N) ratio of the stellar flux:

$$\sigma_{\mathrm{PSF}} = \frac{0.67 \cdot \mathrm{FWHM}}{\mathrm{S/N}}. \tag{3}$$

We measured the FWHM for each OGLE-III subframe and S/N values were estimated using uncertainties of brightness (σ_m [mag]) and the standard relation:

$$\sigma_m = \frac{1.086}{\mathrm{S/N}}. \tag{4}$$

The uncertainty σ_{PSF} reflects only a contribution from a finite number of ADU and nonzero seeing. The total uncertainty of the centroid position also depends on how well one can fit the grid of a given subframe to the grid of the reference subframe. This factor was taken into account later.

Determination of proper motions started with dividing the list of stars from each subfield into subframes in the same manner as in Udalski *et al.* (2008a). This was mandatory as each subframe was reduced separately and the zero point of proper motions may be different. The rest of the calculations were performed for each subframe independently. For each star the time-series astrometry in the pixel scale of the reference image and photometry were obtained from the database of DOPHOT results. Pixel scale was transformed to the equatorial coordinates using transformation for the reference images. For each star and each epoch separately the angles p, z, γ and β were calculated using ephemerides by van Flandern and Pulkkinen (1979). The uncertainties of centroid measurements σ_{PSF} were calculated using Eqs. (3) and (4).

The goal of the following calculations was to find for each epoch and each subframe corrections for positions of centroids that would be used for calculation of proper motions in the reference frame of background objects. By background we assumed 47 Tuc for the field SMC140 and MCs for the remaining fields[‡]. See Anderson and King (2003), Girard *et al.* (2011), van der Marel *et al.* (2002) and Piatek *et al.* (2008) for a discussion of absolute proper motions of background objects. Other important quantities are: correction of centroid uncertainties, dispersion of proper motions of background stars and average $(V-I)$ *vs.* r relations. Accurate calculation of these quantities is possible only if bright stars are taken into account. We selected stars brighter than 18 mag in I-band and with color information (hereinafter "good" stars). For good stars two models were fitted to Eqs. (1) and (2): one with non-zero proper motion (free parameters: α_0, δ_0, μ_α, μ_δ and r) and one with zero proper motions (free parameters: α_0, δ_0 and r). We used the χ^2 minimalization procedure and typically had a few hundred equations (twice the number of centroid measurements for a given star) for five or three unknowns. The nearest stars with significant parallax might have influenced the derived corrections thus at each time we found the proper motions, we excluded the stars with $\mu = \sqrt{\mu_{\alpha\star}^2 + \mu_\delta^2} > 20$ mas/yr, where $\mu_{\alpha\star} = \mu_\alpha \cos\delta$. From the two models we chose the one with non-zero proper motion if resulting χ^2 was smaller than 0.9 times χ^2 for the zero proper motion model. We note that χ^2 values for bright stars were

[‡]Some parts of the SMC131, SMC136 and SMC137 fields are also within the tidal radius of 47 Tuc which equals $42\overset{\prime}{.}9$ (Kiss *et al.* 2007).

much larger than unity, as uncertainties of grid fitting were not included in that iteration. This multiplication constant was changed to 0.95 in the successive iterations. Using the model found this way we calculated expected centroid for each epoch and subtracted it from the observed position. These residua were averaged and their *rms* was found. The average residua were subtracted from the centroids of the given epoch and results were used in the next iteration. The centroid uncertainties $\sigma_{\rm PSF}$ were square added to the *rms* of the residua ($\sigma_{\rm GRID}$) giving uncertainties of centroid positions. These centroids and their uncertainties were used in the next iteration in which all the models were fitted once more. The proper motions were used to find σ-clipped mean proper motion of background stars. The opposite of this proper motion was included into the corrections for positions to assure mean proper motion of background stars would be zero in the next iteration. The *rms* of proper motions of background stars is a measure of our systematic errors and given with subscript *SYS* in the catalog (as opposed to statistical uncertainties derived from χ^2 fitting which are indicated with subscript *STAT*). The χ^2 values of the final fits were close to the unity for most of the stars.

All the above calculations intended to find corrections for positions and their uncertainties, $(V-I)$ *vs.* r relations as well as systematic uncertainties in PMs. Finally, we calculated models with non-zero PM for all stars in a given subframe. We also tried to fit models with parallax but in $\approx 75\%$ of cases the matrix was ill-conditioned. The calculations were also repeated using only exposures with seeing better than 4.5 pix $= 1\farcs17$. This step increased the number of HPM candidates (see below) by 5%. Analysis of the stars with $\mu < 100$ mas/yr will be presented in the forthcoming paper.

Fig. 2 presents the relative histogram of epochs with different $\sigma_{\rm GRID}$ for the LMC and the SMC fields separately. The accuracy of our relative astrometry is typically in the range $2.5 \div 7$ mas which is close to the best wide-field CCD ground-based images. The smallest values of $\sigma_{\rm GRID}$ (below 2 mas) and the tail of the distribution (above 8 mas) were found in the subframes with a small number of good stars. In these subframes our models were poorly constrained. The accuracy of the astrometry in the SMC fields was slightly better than in the LMC fields. Fig. 3 shows the $(V-I)$ *vs.* r relation for two subframes.

The uncertainties of the parallax measurements derived from the least-squares fits ($\sigma_{\pi,\rm LS}$) were unreasonably small – down to 0.12 mas. In order to better assess the quality of our parallax measurements we have searched the whole dataset of our measurements for stars that are present in two adjacent fields, in each of them there were at least 100 epochs and their parallax was greater than 10 mas. For twenty six such pairs we measured the dispersion of differences in π found in both fields and compared it with $\sigma_{\pi,\rm LS}$. This revealed that $\sigma_{\pi,\rm LS}$ are underestimated by 1.5 mas. This component was added in square to each $\sigma_{\pi,\rm LS}$ giving σ_π claimed in the catalog. Parallax value is given only if $\pi/\sigma_\pi > 3$.

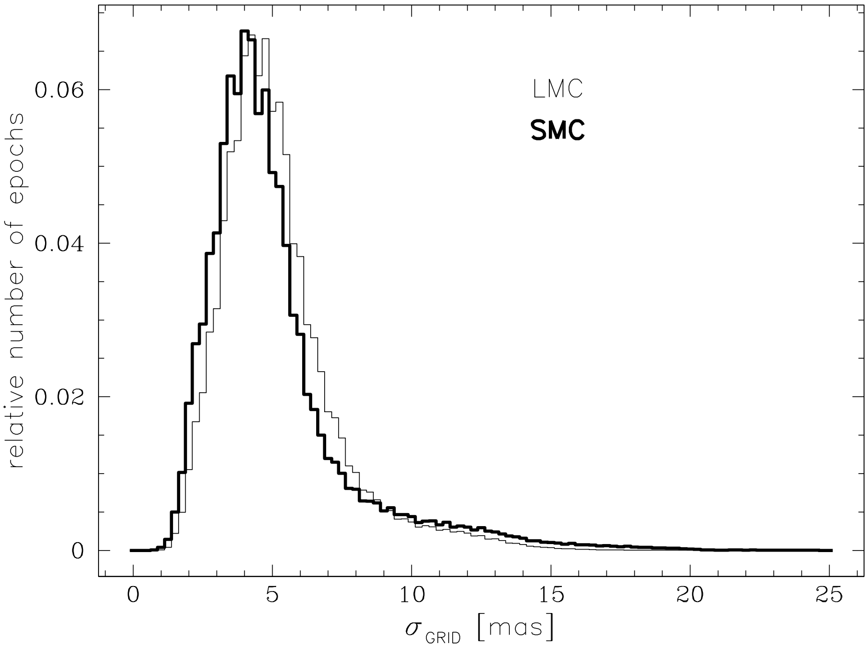

Fig. 2. Relative histogram of $\sigma_{\rm GRID}$ – accuracy with which we fitted grid of the sub-chip to the grid of the reference sub-chip. Thin and thick lines correspond to the LMC and the SMC data, respectively. The bin size is 0.25 mas.

4. Selection of HPM Stars

As HPM stars we defined stars with proper motion greater than 100 mas/yr. We note that stars with $\mu > 126$ mas/yr moved during the OGLE-III time span enough that they may be present in the OGLE-III photometric maps as two separate records. Objects with higher proper motion may have even more records in the database.

We did not use the photometric selection method based on DIA photometry (Eyer and Woźniak 2001). Our tests showed that in the vicinity of bright stars the DIA package produced a higher number of artifacts resembling the HPM photometric behavior. The light curves of some HPM stars did not resemble the expected parabola-like light curves. Both these disadvantages may originate from the fact that our reference images were composed of images taken during long period of time.

To select HPM stars we checked all objects with $\mu > 95$ mas/yr. Most of the objects with the uncertainty of the proper motion $\sigma_\mu > 10$ mas/yr had much less than a hundred measurements and proper motion close to the assumed limit. After inspecting several examples we decided not to analyze these objects, because their number was very high and chances of finding additional sound HPM stars were very low.

The list of candidates selected above was compared with the catalogs presented by Alcock *et al.* (2001) and Soszyński *et al.* (2002). These catalogs con-

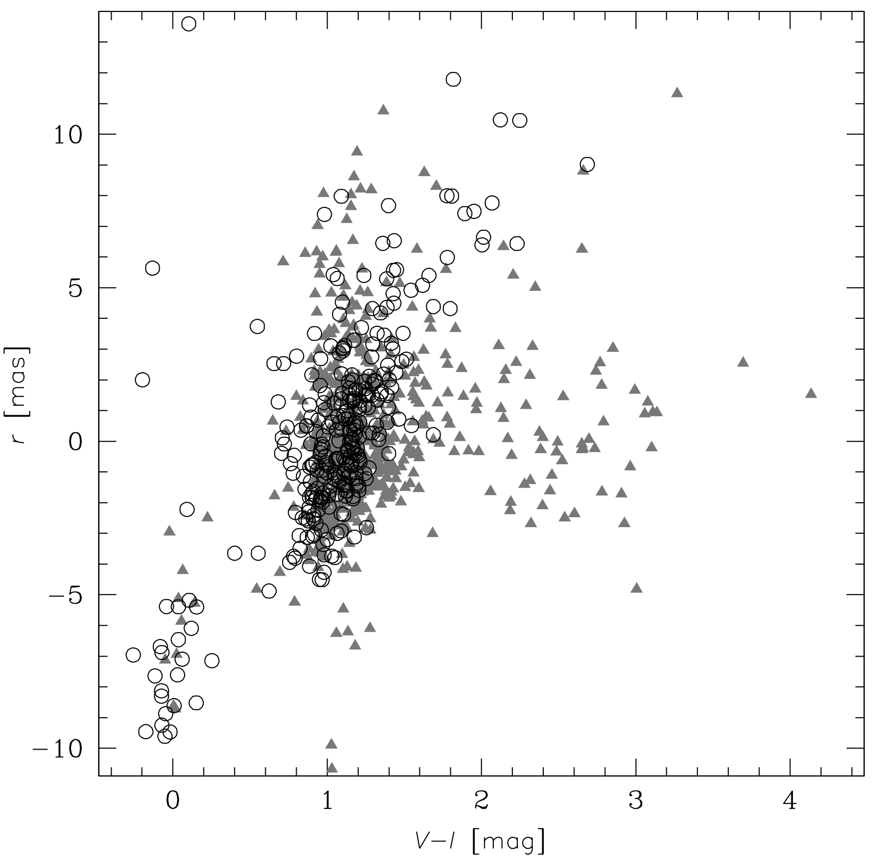

Fig. 3. Differential refraction coefficient r as a function of $V-I$ color for stars in subframes of fields LMC147.3 (black circles) and LMC112.6 (gray triangles).

tain altogether 80 unique stars with $\mu > 95$ mas/yr. Our list of candidates contained 76 of them. Two of the stars (MACHO IDs: 2.4668.10 and 5.5613.1633) were overexposed in the OGLE-III photometry. For the object LMC_SC8 359715 Soszyński *et al.* (2002) gave $\mu = 125.6 \pm 4.0$ mas/yr and our analysis resulted in $\mu = 87.11 \pm 0.67$ mas/yr. The object is present in the two adjacent OGLE-III fields and in both of them consistent results were found. The only one object with $\mu > 95$ mas/yr from the lists of Alcock *et al.* (2001) and Soszyński *et al.* (2002) that was not selected as a candidate HPM was SMC_SC10 57257= 206.16886.2221 with $\mu = 365.01 \pm 0.32$ mas/yr. Its image in the OGLE-III reference frame is so elongated that it was categorized as a diffuse object by the DoPHOT and thus not included in the photometric maps. The OGLE-III identification SMC110.5.999999 was given to that object. We obtained its centroids from the database and analyzed it in the same manner as the other ones. The comparison with the MACHO and OGLE-II catalogs revealed our list of candidates was complete in $76/77 \approx 99\%$.

For some HPM stars we had more than one record in the candidate list from the given field, thus we removed double records from the same field of the same star paying attention not to remove one component of a CPM binary. For each object we scanned the database to find centroids not associated to the object, but localized in a close proximity. This way we increased the number of points used for fitting. Later on, we examined the centroids by eye to remove some of them *e.g.*, measurements with bad seeing, if a HPM was close to another star. The final fit was performed on data acquired this way with corrections described in Section 3. Since the OGLE-III neighboring reference images are overlapping, some objects are present on two, three or even four adjacent fields. For objects selected above we checked if they are present in adjacent fields. If the number of measurements in the second field was significant compared to the number of measurements in the first field, we performed one more fitting. The model contained separate positions for the J2000.0 equinox ($\alpha_{0,1}$, $\delta_{0,1}$ and $\alpha_{0,2}$, $\delta_{0,2}$) and the refraction coefficients (r_1 and r_2) for each field. The values of μ_α, μ_δ and π were kept the same for both fields. This way the number of free parameters increased from six to nine and the number of equations increased as well. The objects with unusually high uncertainties of parameters or large χ^2 values were inspected manually. After calculating the final models, we removed all the HPM candidates with $\mu < 100$ mas/yr leaving 549 objects.

5. Catalog

The catalog of HPM stars contains altogether 551 objects. Two stars have $\mu < 100$ mas/yr but were found to be in CPM binaries with HPM objects. The catalog is available for the astronomical community only in electronic form *via* FTP site:

ftp://ftp.astrouw.edu.pl/ogle/ogle3/pm/hpm_mcs/

For each object we provide the OGLE-III identifier from Udalski *et al.* (2008b, 2008c), equatorial coordinates for J2000.0 equinox from our model fits, proper motion with statistical and systematical uncertainties given separately, parallax, I-band brightness, $V-I$ color and luminosity class (21 WDs, 23 WD candidates and one subdwarf, see Section 5.3). Table 1 shows the exemplary part of the main catalog file. Cross-identifications with MACHO, OGLE-II and SPM4 catalogs are given in a separate file. The brightness estimates differ from those in Udalski *et al.* (2008b, 2008c), firstly, because they were corrected for the differences in transmission between standard and the OGLE-III filters (Szymański *et al.* 2011). Secondly, because a more detailed cross-match between V- and I-band images was performed. For each object a finding chart is also provided with indicated epoch to which it corresponds. We have analyzed the time-series photometry of all cataloged objects and found periodic variability for four of them. The amplitudes are a few hundredths of magnitude and phased light curves show sinusoid-like variability. These together with other comments for a few stars are given in *remarks.txt* file distributed along with the catalog.

T a b l e 1

Exemplary part of the main catalog file

OGLE-III ID	R.A. J2000.0	Dec. J2000.0	$\mu_{\alpha*}$ [mas/yr]	$\sigma_{\mu_{\alpha*},STAT}$ [mas/yr]	$\sigma_{\mu_{\alpha*},SYS}$ [mas/yr]	μ_{δ} [mas/yr]	$\sigma_{\mu_{\delta},STAT}$ [mas/yr]	$\sigma_{\mu_{\delta},SYS}$ [mas/yr]	$\mu=\sqrt{\mu_{\alpha*}^2+\mu_{\delta}^2}$ [mas/yr]	π [mas]	σ_{π} [mas]	I [mag]	σ_I [mag]	$V-I$ [mag]	$\sigma_{(V-I)}$ [mag]	lumin. class
...																
LMC103.7.10025	$5^{h}17^{m}05^{s}.90$	$-69^{\circ}59'06''.0$	82.35	0.13	0.24	221.01	0.13	0.25	235.85	5.03	1.57	16.636	0.012	1.197	0.020	
LMC103.6.78728	$5^{h}17^{m}26^{s}.00$	$-69^{\circ}41'21''.1$	92.92	0.32	0.29	149.81	0.31	0.36	176.29	22.30	1.67	15.088	0.010	2.392	0.017	
LMC105.6.34014	$5^{h}17^{m}57^{s}.55$	$-70^{\circ}54'38''.9$	38.86	0.25	0.24	117.62	0.25	0.19	123.87	9.06	1.73	17.727	0.024	3.143	0.146	
LMC102.7.22769	$5^{h}18^{m}51^{s}.10$	$-68^{\circ}11'17''.7$	−4.67	1.65	0.32	115.80	1.65	0.35	115.89	0.00	0.00	20.033	0.168	0.674	0.206	WDcand
LMC102.7.22886	$5^{h}18^{m}54^{s}.98$	$-68^{\circ}09'48''.3$	0.73	1.44	0.32	121.70	1.44	0.35	121.70	0.00	0.00	19.858	0.147	0.448	0.169	WDcand
LMC103.6.38675	$5^{h}18^{m}58^{s}.18$	$-69^{\circ}47'47''.5$	68.30	0.14	0.31	105.32	0.13	0.36	125.53	11.35	1.57	13.497	0.029	2.120	0.030	
LMC103.3.2	$5^{h}19^{m}08^{s}.19$	$-69^{\circ}48'13''.8$	69.25	0.12	0.26	104.91	0.12	0.25	125.70	12.39	1.55	14.147	0.061	2.559	0.063	
LMC104.4.296	$5^{h}19^{m}42^{s}.85$	$-70^{\circ}14'01''.4$	−72.28	0.22	0.24	287.16	0.22	0.30	296.12	24.72	1.68	17.893	0.028	0.881	0.040	WD
LMC101.3.36262	$5^{h}19^{m}57^{s}.25$	$-68^{\circ}33'04''.5$	−38.19	0.11	0.26	−148.13	0.11	0.33	152.97	7.04	1.54	15.871	0.009	2.195	0.020	
LMC104.1.32254	$5^{h}20^{m}07^{s}.20$	$-70^{\circ}35'31''.7$	−42.97	0.14	0.24	234.53	0.14	0.27	238.43	31.14	1.57	15.823	0.008	2.724	0.026	
LMC101.1.58593	$5^{h}20^{m}10^{s}.21$	$-68^{\circ}52'44''.0$	16.11	1.90	0.47	105.80	1.88	0.36	107.02	0.00	0.00	20.288	0.201	0.686	0.261	WDcand
LMC102.2.30	$5^{h}20^{m}14^{s}.98$	$-68^{\circ}10'07''.9$	−71.53	0.18	0.36	121.56	0.18	0.34	141.04	0.00	0.00	14.859	0.014	1.929	0.021	
LMC102.2.37	$5^{h}20^{m}15^{s}.12$	$-68^{\circ}10'08''.1$	−71.33	0.18	0.36	122.67	0.18	0.34	141.90	4.99	1.60	14.955	0.012	2.093	0.018	
LMC101.2.9556	$5^{h}20^{m}30^{s}.53$	$-68^{\circ}46'32''.3$	25.68	0.11	0.27	106.06	0.11	0.34	109.12	0.00	0.00	14.359	0.016	1.966	0.018	
LMC100.2.19195	$5^{h}20^{m}43^{s}.03$	$-69^{\circ}22'46''.5$	30.73	0.16	0.27	117.17	0.16	0.28	121.13	9.90	1.60	16.481	0.011	2.639	0.041	
LMC106.1.17195	$5^{h}21^{m}26^{s}.11$	$-71^{\circ}49'29''.6$	107.78	0.87	0.32	−52.27	0.87	0.37	119.79	0.00	0.00	19.427	0.098	2.565	0.367	
...																

Luminosity class is given as either WD, WDcand or subdwarf. Main sequence stars are not indicated. One can find three pairs of CPM binaries in the presented list.

The star with the highest detected parallax found is LMC194.6.41 with $\pi = 91.3 \pm 1.6$ mas (*i.e.*, 8.4 times smaller than Proxima Centauri). It is a main sequence star of spectral type $\approx$M5. The highest value of proper motion found was $\mu = 722.19 \pm 0.74$ mas/yr for LMC198.4.97 (*i.e.*, 14.3 times smaller than Barnard's star). Fig. 4 presents equatorial coordinates of LMC194.6.41 and another exemplary star.

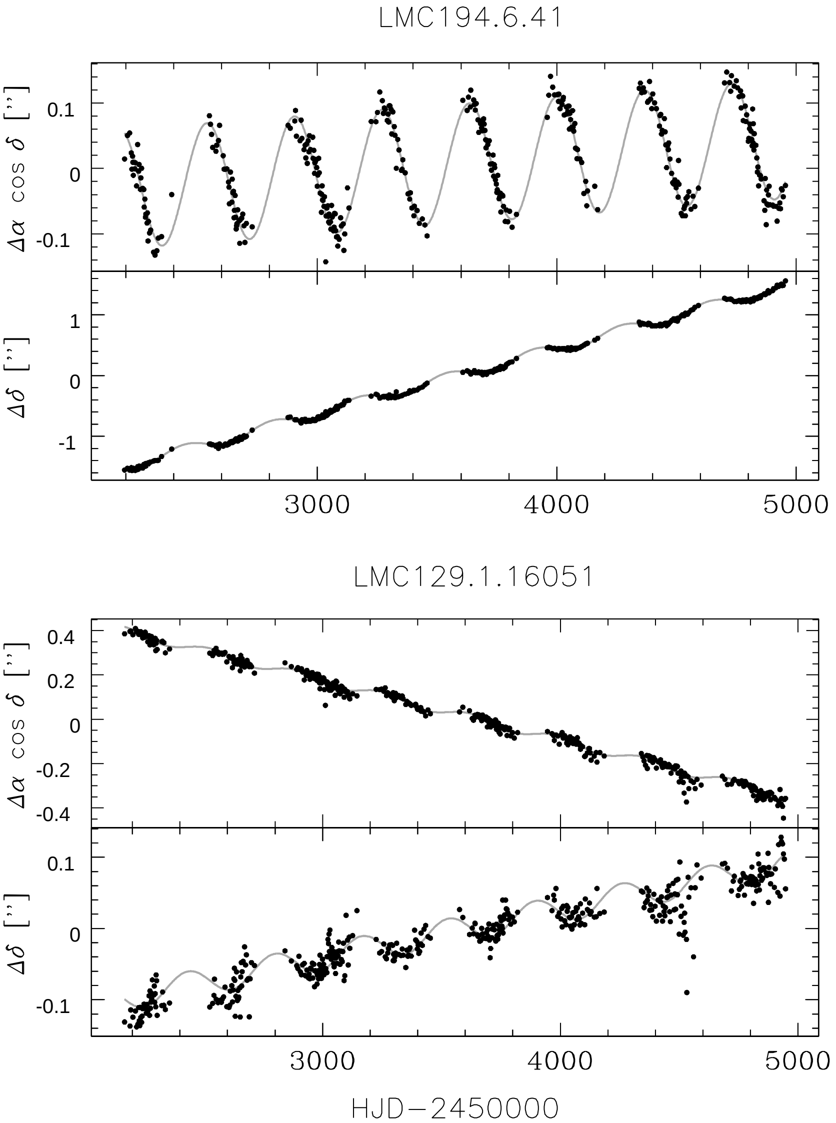

Fig. 4. Equatorial coordinates as a function of time for two exemplary stars with model fits. The differential refraction effect was subtracted from the data. The model parameters $(\mu_{\alpha\star}, \mu_{\delta}, \pi, r)$ are (10.1 mas/yr, 394.6 mas/yr, 91.3 mas, 11.3 mas) for LMC194.6.41 and (−98.2 mas/yr, 24.8 mas/yr, 19.1 mas, 20.2 mas) for LMC129.1.16051.

5.1. Completeness

As was stated earlier we independently found 99% of unique sources from Alcock *et al.* (2001) and Soszyński *et al.* (2002) catalogs with $\mu > 95$ mas. The number of objects in our catalog which are in the sky area covered by OGLE-II and MACHO are 79 and 271, respectively, while these projects found, respectively, 62 and 26 of these objects. Another estimate of the catalog completeness may be performed internally. As mentioned previously some stars are placed on overlapping parts of the frames and we should found such stars independently. For our 551 stars in the catalog we have 584 useful (*i.e.*, with sufficient number of measurements) identifiers in OGLE-III data – 33 stars were present in adjacent subfields. All of them were present on our candidate HPM stars list. It suggests high completeness of the catalog.

The SPM4 catalog (Girard *et al.* 2011) lists 7786 HPM objects located in the MCs OGLE-III fields with *V*-band brightness similar to our stars *i.e.*, between 14 mag and 21 mag. To check reliability of their findings we randomly selected a sample of a hundred stars and retrieved time-series astrometry from the database of raw DoPhot results within a $3''$ radius circle. The plots of $\alpha\cos\delta$ *vs.* δ coordinates with the color-coded epoch of measurements were examined in detail. Only eight of these plots showed clearly moving objects. Two of them are in our catalog and for other six the inferred proper motions are below 50 mas/yr. We conclude that the reliability of SPM4 catalog in MCs sky area is not sufficient to compare it with our list.

Fig. 5 shows sky projection of the HPM stars found. No obvious correlation between the number of background stars and the number of HPM stars can be seen, though, some regions, like Tarantula Nebula (field LMC175) and the center of the SMC (field SMC100) show smaller number of HPM stars. We used the Besançon Milky Way model (Robin *et al.* 2003) to find the expected number of HPM stars in the *I*-band brightness range $12.8 \div 20.2$ mag. For the center of the LMC the model estimate was 4.3 HPM stars per area equivalent to the OGLE-III field. For the SMC the number was 4.7. If compared to the observed numbers: 3.4 and 4.6 for the LMC and SMC, respectively, this gave estimated completeness of 79% and 98%. The biggest difference which plausibly increases the completeness in the SMC fields as compared to the LMC fields was the larger number of epochs in the SMC fields, but we do not think this could so much influence the completeness. No other effect which may result in such a discrepancy was found except possible small structures in the local number density of stars which are not well characterized in the Besançon model.

5.2. Comparison with OGLE-II and MACHO Catalogs

While comparing the derived proper motions one has to keep in mind that if the results in the two catalogs are based on images obtained a few years apart, the blending with different background stars can be the main cause of differences in

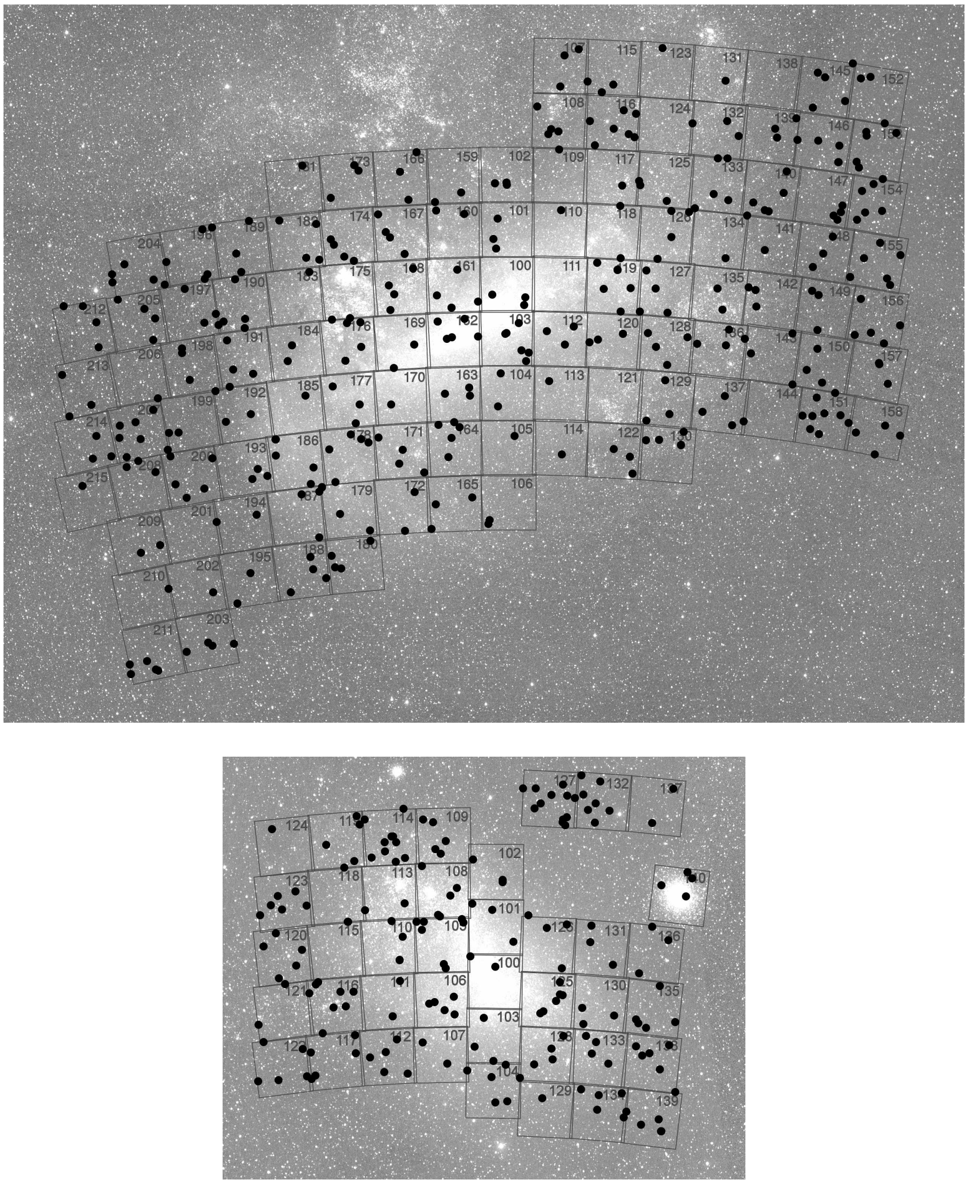

Fig. 5. Positions of HPM stars found (black dots) in the foreground of the LMC (*upper panel*) and SMC (*lower panel*). Squares mark the borders of OGLE-III fields with number given inside. The background images originate from the ASAS survey (Pojmański 1997).

the results. The blending is more probable in the dense stellar regions and indeed we see the biggest differences for stars located in the densest fields. Our catalog has 62 (26) common records with OGLE-II (MACHO) catalog. After removing the most outlying results, we were left with the *rms* of proper motion per coordinate differences equal to 3.3 mas/yr for OGLE-II and 5.9 mas/yr for MACHO catalog. Using OGLE-II and our error bars we estimated the expected *rms* of 1.7 mas/yr.

For MACHO proper motions Alcock *et al.* (2001) only gave typical uncertainty of roughly 3.5 mas/yr per coordinate. There are eleven stars for which both we and Soszyński *et al.* (2002) gave estimates of parallax. Our results are on average 2.5 ± 1.0 mas greater and the average uncertainty of our measurements is 1.6 mas.

5.3. Color–Magnitude Diagram

For stars with parallax measurements we calculated the absolute magnitudes in the *I*-band (M_I). They are shown as a function of $V - I$ color in Fig. 6. The error-bars in M_I include uncertainties of the *I*-band photometry and parallax measurements. The points close to the lower right corner have large $V - I$ error-bars because they are close to the detection limit in the *V*-band. One can clearly see the main sequence stars most of which have $(V - I) > 2$ mag. The bluest objects (light blue triangles in Fig. 6) are WDs which well separate from the main sequence stars. Between these two groups there is a dozen or so stars which may be candidate subdwarfs, although, all of them except one object (SMC110.5.999999; $(V - I) = 1.51$ mag, $M_I = 12.1$ mag) have poorly known absolute magnitudes and it is hard to select a clear sample of subdwarfs without additional observations. Altogether 365 points are shown in Fig. 6; 20 objects were rejected because their $V - I$ color is not known. Among 385 stars with parallax measured the one with the faintest absolute brightness is SMC108.6.8038 ($M_I = 18.08 \pm 0.35$ mag).

Fig. 7 shows the CMD for all HPM stars with color information. The stars with parallax measured are shown using the same symbols as in Fig. 6. The stars without parallax measured are shown using dark blue symbols, if they are fainter or bluer than the locus of WDs from Fig. 6, and red dots otherwise. These objects (dark blue symbols) are classified as WD candidates. The red points indicate stars which most probably are main sequence stars which are farther away than the stars marked with black points.

5.4. Common Proper Motion Binaries

The list of confirmed stars with $\mu > 95$ mas/yr was cross-matched with itself and the pairs of stars located less than $5'$ from each other were checked if the values and the directions of their proper motions are similar. Table 2 presents the list of 27 CPM binaries in which at least one component had $\mu > 100$ mas/yr. Six of these binaries are uncertain. The separation of the components ranges from $0\farcs7$ to $144\farcs3$. Large difference in brightness between components of CPM binary suggests the fainter object may have very faint absolute brightness. We indicated the difference in the *I*-band brightness, if it was larger than 3.5 mag.

6. Summary

The presented catalog contains 549 stars with $\mu > 100$ mas/yr observed in the direction to the Magellanic Clouds, which are dense stellar regions. The highest

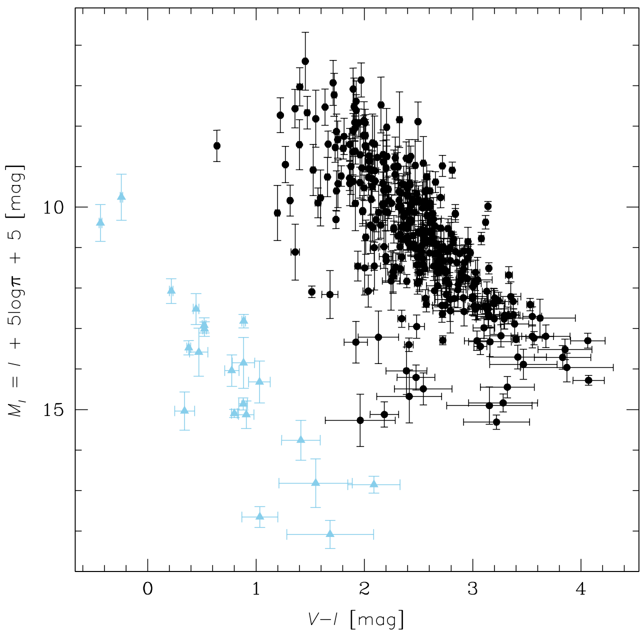

Fig. 6. Color–absolute magnitude diagram for stars with measured parallax. WDs are marked with light blue triangles.

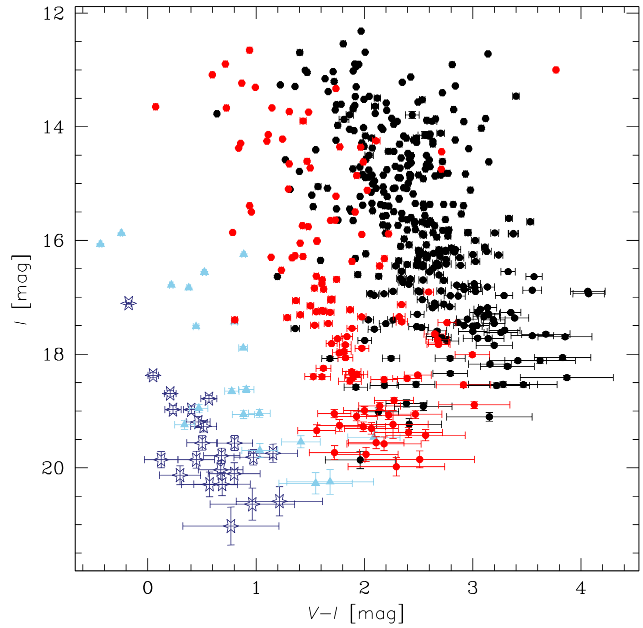

Fig. 7. Color–magnitude diagram. Black and light blue symbols show the same stars as in Fig. 6. Dark blue symbols indicate candidate WDs and red dots indicate all other stars without parallax measured.

Table 2

Common proper motion binaries

ID1	ID2	angular dist. [″]	μ [mas/yr]	comments
LMC162.4.41184	LMC162.4.41229	0.7	151	
LMC102.2.30	LMC102.2.37	0.9	141	
LMC130.3.25	LMC130.3.4226	1.2	107	
LMC120.6.17556	LMC120.6.17583	1.4	168	
LMC179.4.38816	LMC179.4.40244	1.4	111	uncertain; $\Delta I = 4.7$ mag
SMC125.7.29221	SMC125.7.29234	1.7	124	
LMC174.8.25010	LMC174.8.31202	2.9	102	$\Delta I = 3.6$ mag
SMC111.8.20419	SMC111.8.20441	3.7	102	
LMC146.8.30	LMC146.8.31	3.7	106	
LMC155.1.4867	LMC155.1.5999	3.7	100	
SMC133.4.124	SMC133.4.3322	3.9	106	uncertain
LMC166.5.30	LMC166.5.499	4.1	205	
LMC161.1.38	LMC161.1.5	6.5	113	
LMC126.1.100	LMC126.1.9	6.6	127	
LMC176.1.34425	LMC176.1.34431	6.7	111	
SMC139.7.1569	SMC139.7.1570	8.2	103	
LMC119.5.40603	LMC119.5.40836	8.2	144	
SMC115.5.12	SMC115.5.319	9.1	315	$\Delta I = 3.8$ mag
LMC130.6.186	LMC130.6.29	10.6	151	uncertain
LMC186.4.38205	LMC186.4.38233	16.0	181	uncertain
SMC110.8.23710	SMC110.8.23860	19.0	180	
LMC103.3.2	LMC103.6.38675	58.3	126	
SMC114.6.11666	SMC114.7.14379	65.2	113	
SMC125.6.4503	SMC125.6.8973	86.0	126	uncertain
LMC102.7.22769	LMC102.7.22886	92.0	119	
LMC211.1.10	LMC211.8.3926	114.3	208	
LMC106.1.14252	LMC106.1.17195	147.3	115	uncertain

The brightness difference ΔI is given if larger than 3.5 mag.

proper motion found is 722.19 ± 0.74 mas/yr. For 70% of these objects parallaxes were measured with significance greater than 3σ. The closest object has $\pi = 91.3 \pm 1.6$ mas. The completeness of the catalog is higher by at least 27% than the previous ones investigating the same sky area. Altogether 44 objects are marked as WDs or candidate WDs.The search for CPM binaries resulted in 27 pairs. The catalog may be useful for estimation of the local number density of intrinsically faint objects. The follow-up observations in the infrared or cross-matching with existing catalogs may result in a candidate brown dwarfs in the close proximity of our HPM. The MCs host many different types of astrophysically important objects and are the nearest such galaxies, thus follow-up observations may be performed when other targets are observed. Jointly with other catalogs this may extend further our knowledge of the Galaxy dynamics, the motion of the Sun against nearby stars and wide binary systems.

The uncertainties of our proper motions are around 0.5 mas/yr. Our results were compared to the other catalogs and the major contribution to differences found came from blending of the HPM stars with different objects in different surveys. The catalog of stars with $\mu < 100$ mas/yr toward the MCs will be presented in the forthcoming paper. A continuation of our efforts will be a calculation of proper motions in the OGLE-III Galactic Bulge fields.

Acknowledgements. Authors thank S. Kozłowski and P. Pietrukowicz for comments on manuscript. This work was supported by MNiSW grant N-N203-512538. RP is supported through Polish Science Foundation START program. The OGLE project has received funding from the European Research Council under the European Community's Seventh Framework Programme (FP7/2007-2013)/ERC grant agreement No. 246678.

REFERENCES

Alard, C., and Lupton, R.H. 1998, *ApJ*, **503**, 325.
Alard, C. 2000, *A&AS*, **144**, 363.
Alcock, C., *et al.* 2001, *ApJ*, **562**, 337.
Anderson, J., Bedin, L.R., Piotto, G., Yadav, R.S., and Bellini, A. 2006, *A&A*, **454**, 1029.
Anderson, J., and King, I.R. 2003, *AJ*, **126**, 772.
Eyer, L., and Woźniak, P.R. 2001, *MNRAS*, **327**, 601.
Finch, C.T., Henry, T.J., Subasavage, J.P., Jao, W.-C., and Hambly, N.C. 2007, *AJ*, **133**, 2898.
Girard, T.M., *et al.* 2011, *AJ*, **142**, 15.
Kiss, L.L., Székely, P., Bedding, T.R., Bakos, G.Á., and Lewis, G.F. 2007, *ApJ*, **659**, 129.
Kozłowski, S., Woźniak, P.R., Mao, S., Smith, M.C., Sumi, T., Vestrand, W.T., and Wyrzykowski, Ł. 2006, *MNRAS*, **370**, 435.
Kuijken, K., and Rich, R.M. 2002, *AJ*, **124**, 2054.
Piatek, S., Pryor, C., and Olszewski, E.W. 2008, *AJ*, **135**, 1024.
Pojmański, G. 1997, *Acta Astron.*, **47**, 467.
Robin, A.C., Reylé, C., Derriére, S., and Picaud, S. 2003, *A&A*, **409**, 523.
Schechter, P.L., Mateo, M., and Saha, A. 1993, *PASP*, **105**, 1342.
Skrutskie, M.F., *et al.* 2006, *AJ*, **131**, 1163.
Soszyński, I., Żebruń, K., Udalski, A., Woźniak, P.R., Szymański, M., Kubiak, M., Pietrzyński, G., Szewczyk, O., and Wyrzykowski, Ł. 2002, *Acta Astron.*, **52**, 143.
Soszyński, I., Udalski, A., Szymański, M.K., Kubiak, M., Pietrzyński, G., Wyrzykowski, Ł., Szewczyk, O., Ulaczyk, K., and Poleski, R. 2009, *Acta Astron.*, **59**, 1.
Szymański, M.K., Udalski, A., Soszyński, I., Kubiak, M., Pietrzyński, Poleski, R., Wyrzykowski, Ł., and Ulaczyk, K. 2011, *Acta Astron.*, **61**, 83.
Udalski, A. 2003, *Acta Astron.*, **53**, 291.
Udalski, A., Szymański, M.K., Soszyński, I., and Poleski, R. 2008a, *Acta Astron.*, **58**, 69.
Udalski, A., Soszyński, I., Szymański, M.K., Kubiak, M., Pietrzyński, G., Wyrzykowski, Ł., Szewczyk, O., Ulaczyk, K., and Poleski, R. 2008b, *Acta Astron.*, **58**, 89.
Udalski, A., Soszyński, I., Szymański, M.K., Kubiak, M., Pietrzyński, G., Wyrzykowski, Ł., Szewczyk, O., Ulaczyk, K., and Poleski, R. 2008c, *Acta Astron.*, **58**, 329.
van der Marel, R.P., Alves, D.R., Hardy, E, and Suntzeff, N.B. 2002, *AJ*, **124**, 2639.
van Flandern, T.C., and Pulkkinen, K.F. 1979, *ApJS*, **41**, 391.
Woźniak, P.R. 2000, *Acta Astron.*, **50**, 421.
Zacharias, N., *et al.* 2010, *AJ*, **139**, 2184.